© 2015. Published by The Company of Biologists Ltd | Development (2015) 142, 218-228 doi:10.1242/dev.114769

RESEARCH ARTICLE

Nesprins anchor kinesin-1 motors to the nucleus to drive nuclear distribution in muscle cells

Meredith H. Wilson and Erika L. F. Holzbaur*

ABSTRACT

During skeletal muscle development, nuclei move dynamically through myotubes in a microtubule-dependent manner, driven by the microtubule motor protein kinesin-1. Loss of kinesin-1 leads to improperly positioned nuclei in culture and *in vivo*. Two models have been proposed to explain how kinesin-1 functions to move nuclei in myotubes. In the cargo model, kinesin-1 acts directly from the surface of the nucleus, whereas in an alternative model, kinesin-1 moves nuclei indirectly by sliding anti-parallel microtubules. Here, we test the hypothesis that an ensemble of Kif5B motors acts from the nuclear envelope to distribute nuclei throughout the length of syncytial myotubes. First, using an inducible dimerization system, we show that controlled recruitment of truncated, constitutively active kinesin-1 motors to the nuclear envelope is sufficient to prevent the nuclear aggregation resulting from depletion of endogenous kinesin-1. Second, we identify a conserved kinesin light chain (KLC)-binding motif in the nuclear envelope proteins nesprin-1 and nesprin-2, and show that recruitment of the motor complex to the nucleus via this LEWD motif is essential for nuclear distribution. Together, our findings demonstrate that the nucleus is a kinesin-1 cargo in myotubes and that nesprins function as nuclear cargo adaptors. The importance of achieving and maintaining proper nuclear position is not restricted to muscle fibers, suggesting that the nesprin-dependent recruitment of kinesin-1 to the nuclear envelope through the interaction of a conserved LEWD motif with kinesin light chain might be a general mechanism for cell-type-specific nuclear positioning during development.

KEY WORDS: Cargo adaptor, Kinesin-1, Muscle development, Nesprin, Nuclear positioning, Mouse

INTRODUCTION

The position of the nucleus in a cell is dynamically controlled by interactions between the nuclear envelope (NE) and the cytoskeleton. Defects in nuclear positioning are often associated with cellular dysfunction and human disease, including muscular dystrophy, cardiomyopathy, lissencephaly and hearing loss (Gundersen and Worman, 2013). Proper nuclear positioning is especially crucial in skeletal muscle cells. Skeletal muscle fibers are large multinucleated cells formed by the fusion of post-mitotic myoblasts. The nuclei in mature muscle fibers are anchored under the sarcolemma at the cell periphery, and positioned to maximize internuclear distances, thereby minimizing transport distances from nucleus to cytoplasm (Bruusgaard et al., 2003). Abnormal aggregation or mispositioning of nuclei noted in many muscle diseases (Mattioli et al., 2011; Romero, 2010) correlates with muscle weakness and dysfunction observed in model organisms (Metzger et al., 2012; Wang et al., 2013a), suggesting that normal nuclear positioning is required for proper muscle cell function.

During skeletal muscle development, nuclei move dynamically through the cell in a microtubule-dependent manner (Englander and Rubin, 1987; Wilson and Holzbaur, 2012). These dynamics include translocation as well as rotation in three dimensions (Capers, 1960; Wilson and Holzbaur, 2012); both are attenuated by depolymerization of the microtubule network (Englander and Rubin, 1987; Wilson and Holzbaur, 2012). Recent progress indicates that the microtubule motor proteins kinesin-1 (Kif5B) and cytoplasmic dynein power nuclear dynamics (Cadot et al., 2012; Folker et al., 2012, 2014; Metzger et al., 2012; Wilson and Holzbaur, 2012). Loss of either the plus-end-directed kinesin-1 motor or the minus-end-directed dynein motor leads to reduced rates of translocation and rotation, although the effects are more pronounced in myotubes depleted of kinesin-1 (Wilson and Holzbaur, 2012). Furthermore, loss of Kif5B causes dramatic aggregation of nuclei at the midline of the cell in cultured mouse myotubes (Metzger et al., 2012; Wilson and Holzbaur, 2012), and *in vivo* in fly and mouse muscles (Metzger et al., 2012; Wang et al., 2013a).

Two models have been proposed to explain how Kif5B functions to move nuclei in myotubes. In the model proposed by Metzger et al. (2012), Kif5B interacts with the microtubule-associated protein MAP7/ensconsin to slide anti-parallel microtubules, thereby pushing adjacent nuclei apart (Fig. 1A). Alternatively, we proposed that Kif5B acts from the nuclear surface, moving the nucleus as a giant cargo along the local microtubule network (Wilson and Holzbaur, 2012) (Fig. 1A).

Kinesin-1 is a heterotetramer, composed of a dimer of Kif5 kinesin heavy chains (KHCs) and two regulatory kinesin light chains (KLCs). In a number of cell types, including *C. elegans* hypodermal precursor cells (Meyerzon et al., 2009) and mammalian epithelial cells (Horn et al., 2013; Roux et al., 2009; Schneider et al., 2011), KLC mediates the association of KHC with the NE through interactions with members of the KASH (Klarsicht, ANC-1, SYNE homology) family of proteins. These proteins, including the vertebrate nesprins, interact via their KASH domain with SUN (Sad1, UNC-84) proteins that span the inner nuclear membrane and associate with the nuclear lamina (Starr and Fridolfsson, 2010). Although KLC is localized to the NE in mammalian cells (Wilson and Holzbaur, 2012), KLC mutants in *Drosophila* do not show defects in myonuclear positioning (Metzger et al., 2012), raising questions about the role of KLC in anchoring Kif5B to the NE in muscle.

Evidence from knockout mice suggests that nesprin-1 and nesprin-2 are crucial for nuclear positioning in both skeletal muscle and cardiomyocytes (Banerjee et al., 2014; Chapman et al., 2014; Zhang et al., 2010, 2007b). Moreover, mutations in both nesprin-1 and nesprin-2 are found in individuals with Emery–Dreifuss muscular dystrophy (Zhang et al., 2007a), which is characterized by progressive skeletal muscle weakness and

Department of Physiology and the Pennsylvania Muscle Institute, Perelman School of Medicine, University of Pennsylvania, Philadelphia, PA 19104, USA.

*Author for correspondence (holzbaur@mail.med.upenn.edu)

Received 25 June 2014; Accepted 9 November 2014

Development (2015) 142, 218-228 doi:10.1242/dev.114769

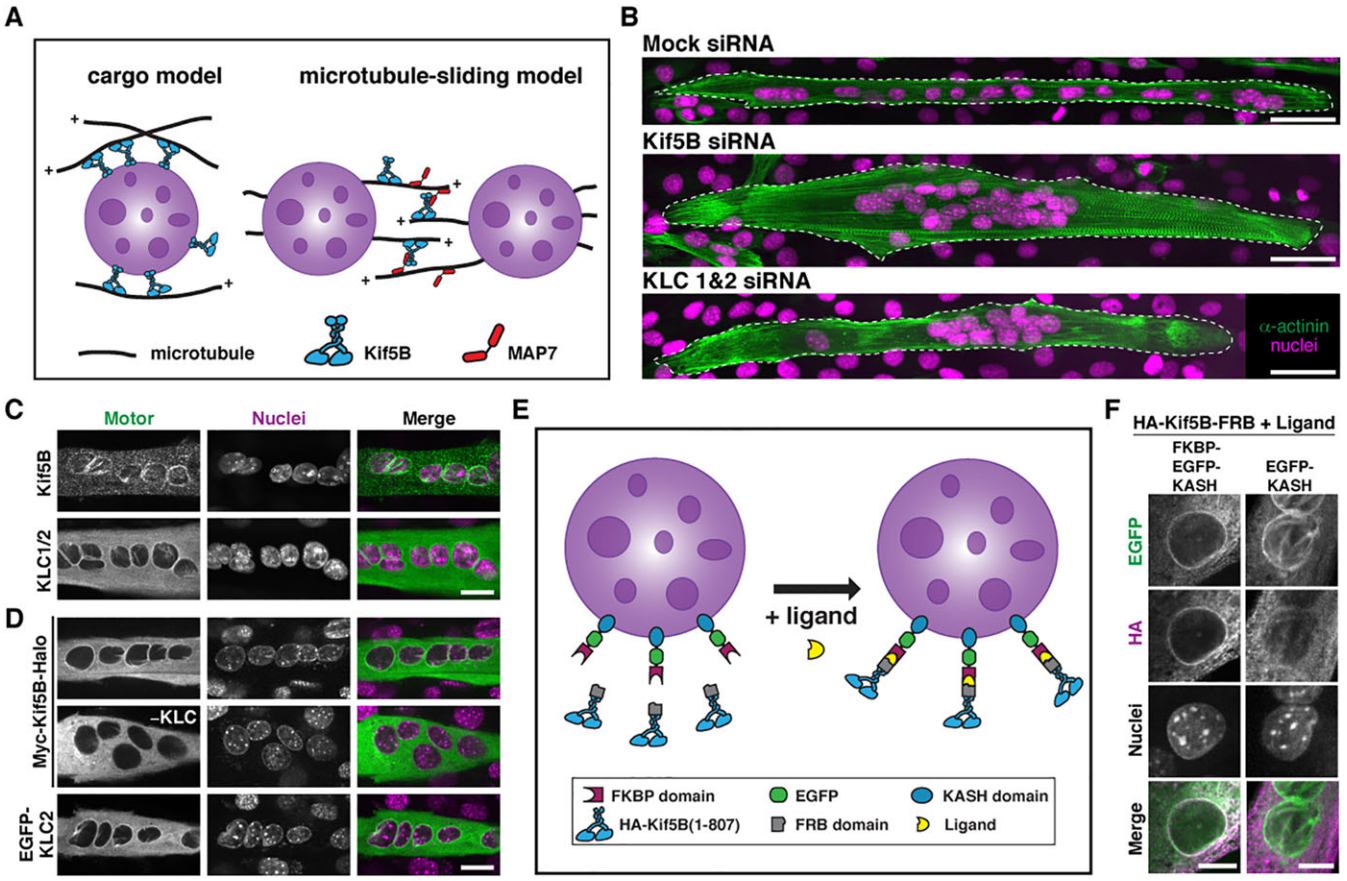

Fig. 1. Design of Kif5B recruitment system. (A) Proposed models of Kif5B-dependent nuclear movement in myotubes. (B) Representative images of C2C12 myotubes treated with siRNA to Kif5B, to kinesin light chains 1 and 2 or mock transfected. Nuclei were stained with Hoechst dye (magenta); α-actinin is in green. Images are maximum projections of confocal *z*-sections. Scale bars: 50 µm. (C) Myotubes were immunostained for Kif5B heavy chain (mAb SUK4) or KLC1 and KLC2 (mAb 63-90); nuclei are labeled with Hoechst dye. Scale bar: 20 µm. (D) Myotubes were either transfected with Myc-Kif5B-Halo and labeled with Halo-TMR ligand, or transfected with EGFP-KLC2 with or without siRNA to KLC1 and KLC2. Scale bar: 20 µm. (E) Fusion constructs for induced recruitment of truncated Kif5B to the nucleus. FKBP-EGFP-KASH targets the NE; HA-Kif5B(1-807)-FRB motor constructs are cytosolic. Following ligand addition, heterodimerization of FKBP-FRB domains anchors constitutively active Kif5B(1-807) to the NE. (F) Nuclei in myotubes expressing FKBP-EGFP-KASH recruit HA-Kif5B(1-807)-FRB to the nuclear surface with ligand treatment, whereas nuclei coated with EGFP-KASH do not recruit the motor construct. Myotubes were immunostained for HA and EGFP. Scale bars: 10 µm. See also supplementary material Fig. S1 for additional data.

cardiomyopathy. These findings suggest that nuclear position is essential for normal muscle function, and that an interaction between kinesin-1 and nesprins may facilitate the nuclear dynamics necessary to position myonuclei.

Here, we use multiple experimental strategies to test the cargo model of Kif5B-dependent nuclear positioning in myotubes. We show that controlled recruitment of a truncated, constitutively active Kif5B motor to the NE is sufficient to prevent the nuclear aggregation resulting from depletion of endogenous Kif5B. We identify a conserved KLC-binding motif in nesprin-1 and nesprin-2, and show that this motif is necessary for the localization of kinesin-1 motors to the nuclear membrane. Finally, depletion of either KLC or nesprins results in nuclear aggregation at the midline of the myotube that can be rescued with wild-type constructs but not by constructs with mutations that disrupt the KLC-nesprin interaction. Together, our results support the model that kinesin-1 acts from the NE to drive the distribution of nuclei in myotubes.

RESULTS

Recruitment of exogenous Kif5B to the nuclear envelope rescues nuclear distribution in myotubes

In C2C12 myotubes, treatment with siRNA to Kif5B kinesin heavy chain (KHC) results in dramatic aggregation of nuclei at the mid-line of the cell (Fig. 1B). Nuclear aggregation is also prominent in myotubes treated with siRNA to both KLC1 and KLC2 (Fig. 1B; supplementary material Fig. S1). Depletion of Kif5B (to 31±5% of mock, mean±s.d., n=3) results in concomitant depletion of KLC1 and KLC2 (supplementary material Fig. S1), as previously noted in primary mouse myotubes generated from Kif5B conditional knockout mice (Wang et al., 2013a). Similarly, siRNA-mediated depletion of KLC (to 3±2% of mock, mean±s.d., n=3) also reduces levels of Kif5B, consistent with coordinate regulation of KHC and KLC expression levels.

Endogenous Kif5B and KLC accumulate at the NE in myotubes (Wilson and Holzbaur, 2012) (Fig. 1C). Myc-Kif5B-Halo and EGFP-KLC2 constructs also localize to myotube nuclei in live cell assays (Fig. 1D). However, Myc-Kif5B-Halo is not recruited to the NE in myotubes treated with siRNA to KLC1 and KLC2 (Fig. 1D), suggesting that KLC mediates the recruitment of KHC to nuclei in mammalian myotubes.

To test the hypothesis that Kif5B acts from the nuclear surface to drive nuclear movement, we used an inducible cargo trafficking assay (Kapitein et al., 2010a,b) to recruit Kif5B motors to the NE (Fig. 1E). In this system the ligand-mediated heterodimerization of FKBP and FRB protein domains is induced by the cell-permeant ligand rapalog (Clackson et al., 1998; Spencer et al., 1993). By targeting the FKBP

Development (2015) 142, 218-228 doi:10.1242/dev.114769

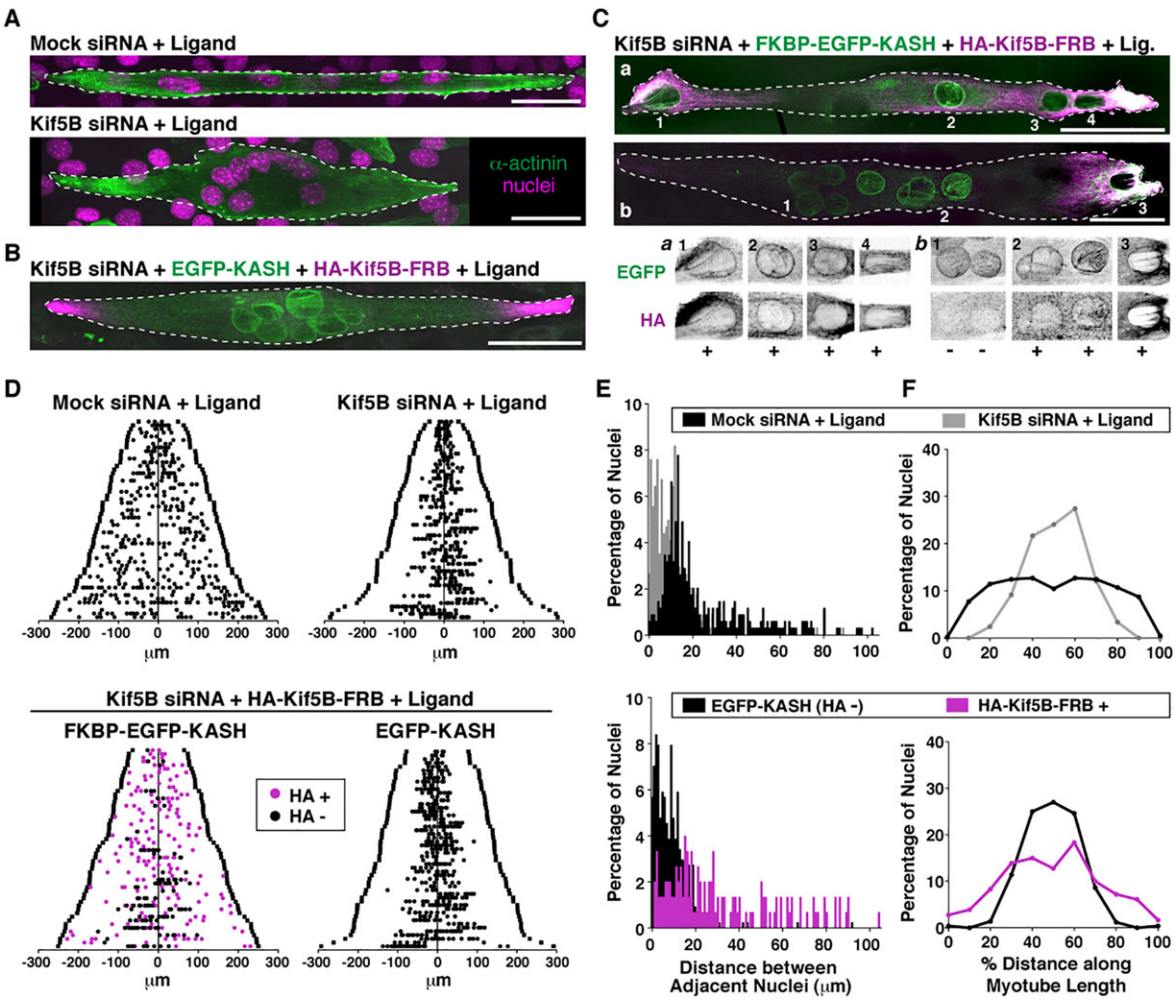

Fig. 2. Recruitment of exogenous Kif5B to the nuclear envelope rescues nuclear distribution in myotubes. (A) Representative images showing normal nuclear distribution in mock-treated cells versus nuclear aggregation in Kif5B siRNA-treated myotubes that were also treated with ligand. Images are maximum projections of confocal *z*-sections. Scale bars: 50 µm. (B) Nuclei in Kif5B siRNA-treated myotubes expressing EGFP-KASH do not recruit HA-Kif5B (1-807)-FRB to the NE and aggregate at the cell midline, despite ligand treatment. Fixed myotubes were immunostained for EGFP and HA; constitutively active HA-Kif5B(1-807)-FRB tends to accumulate near plus-ends of microtubules at myotube ends. Scale bar: 50 µm. (C) Examples of Kif5B siRNA-treated myotubes co-expressing FKBP-EGFP-KASH and HA-Kif5B(1-807)-FRB. With ligand treatment, all nuclei become HA+ in some myotubes (a,a′), whereas in other cells, only a subset of nuclei recruit the motor (b,b′). Lower panels show inverted grayscale images of the numbered nuclei in the top panels. Scale bars: 50 µm. Nuclei were individually evaluated for recruitment of HA-Kif5B(1-807)-FRB to the NE by quantitative line scan analysis. Plus and minus marks indicate the designation of a particular nucleus as HA+ or HA–. For more details, see supplementary material Fig. S2. Only HA+ nuclei show normal nuclear distribution. (D) Distribution of nuclei in treated myotubes. Each line on the *y*-axis represents an individual myotube, organized according to length (*n*=53-56 myotubes). The ends of the myotube are marked by a dark square; data points represent individual nuclei. HA-Kif5B(1-807)-FRB-decorated nuclei are magenta. (E) Frequency distributions of the distance between adjacent nuclei in treated myotubes (1 µm bin width; less than 2.5% of all the data lies above 105 µm so distributions are truncated for clarity). (F) Histograms depicting nuclear position as a percentage of distance along the myotube (bin width=10%). See supplementary material Fig. S2 for additional controls.

domain to a cargo of interest and the FRB domain to an active motor construct, ligand treatment induces controlled motor recruitment to the cargo. First, we verified the feasibility of this system in C2C12 myotubes by inducing recruitment of HA-Kif5B(1-807)-FRB to FKBP-decorated peroxisomes. Truncated Kif5B(1-807) lacks the tail domain, preventing association of the motor with many endogenous cargoes, and also preventing autoinhibition induced by tail binding to the motor domains of the KHC dimer (Kaan et al., 2011; Verhey and Hammond, 2009; Verhey et al., 1998). With ligand addition, we observed directed motility of peroxisomes toward the plus-ends of microtubules and accumulation of peroxisomes at the ends of the myotube, indicating successful ligand-mediated recruitment of constitutively active HA-Kif5B(1-807)-FRB motors to these organelles (supplementary material Fig. S1).

Next, we adapted the system for controlled recruitment of HA-Kif5B(1-807)-FRB to the NE. We fused the FKBP domain to the C-terminal transmembrane and KASH domains of the NE protein nesprin-2 (FKBP-EGFP-KASH) (Fig. 1E). Using this strategy, we found that FKBP-EGFP-KASH and a control construct lacking the FKBP domain (EGFP-KASH) both localized to the NE in myotubes. With ligand treatment, only nuclei decorated with FKBP-EGFP-KASH successfully recruited HA-Kif5B-FRB to their surface (Fig. 1F); ligand treatment alone did not affect myotube morphology or differentiation (Fig. 2A; also see supplementary material Fig. S2).

To test the hypothesis that kinesin acts from the nuclear surface to distribute nuclei properly in myotubes, we depleted endogenous Kif5B with siRNA and used our inducible heterodimerization system to selectively restore constitutively active kinesin motors to the NE.

Development (2015) 142, 218-228 doi:10.1242/dev.114769

If Kif5B is required on the nuclear envelope, only nuclei decorated with HA-Kif5B-FRB should escape central aggregation and display proper distribution throughout the myotube. As expected, nuclei in mock siRNA-treated myotubes were distributed throughout the length of the cell, whereas nuclei in Kif5B siRNA-treated myotubes aggregated at the midline (Fig. 2A,D,F). When the HA-Kif5B-FRB was co-expressed with the control EGFP-KASH construct lacking the FKBP domain in Kif5B siRNA-treated myotubes, ligand treatment did not induce recruitment of kinesin to the NE (Fig. 2B). Nuclei in these myotubes remained aggregated at the cell center (Fig. 2B,D,F), indicating that cytosolic HA-Kif5B-FRB was not sufficient to rescue nuclear distribution.

By contrast, in Kif5B siRNA-treated myotubes co-expressing HA-Kif5B-FRB and FKBP-EGFP-KASH, treatment with the heterodimerizing ligand induced recruitment of the motor to the NE (Fig. 2C). Recruitment of HA-Kif5B-FRB was independently evaluated for each nucleus by quantitative line scan analysis (see supplementary material Fig. S2). In over 60% of cells, all nuclei successfully recruited HA-Kif5B-FRB (Fig. 2Ca,a′), while in the remaining 40% only some nuclei were decorated (Fig. 2Cb,b′). In both populations, HA-Kif5B-FRB-positive nuclei were distributed throughout the length of the myotubes (Fig. 2C; magenta circles in Fig. 2D,F), while nuclei lacking detectable levels of HA-Kif5B-FRB remained aggregated at the cell center (black circles in Fig. 2D; FKBP-EGFP-KASH plot).

In myotubes deficient for endogenous Kif5B, the distance between adjacent nuclei was significantly smaller than in mock siRNA-treated myotubes (11±13 µm, n=416 nuclei in 56 myotubes versus 28±30 µm, 402 nuclei in 54 myotubes, respectively, mean±s.d., P<0.001; Kruskal–Wallis with Dunn's post-hoc test; see frequency distributions in Fig. 2E). The distance between adjacent nuclei was similarly reduced in Kif5B siRNA-treated myotubes co-expressing EGFP-KASH and HA-Kif5B-FRB (10±15 µm, n=500 nuclei in 53 myotubes; P<0.001 versus mock siRNA). However, the mean distance between adjacent nuclei decorated with HA-Kif5B-FRB was significantly higher than the distance between nuclei in the mock siRNA-treated myotubes (42±46 µm; n=180 nuclei in 54 myotubes; P<0.001). Strikingly, HA-Kif5B-FRB-positive nuclei were often at the extreme ends of the myotubes (Fig. 2C,D,F), an area enriched in microtubule plus-ends (Wilson and Holzbaur, 2012). These findings are consistent with the cargo model of Kif5B-dependent nuclear movement in myotubes and suggest that the constitutively active Kif5B construct may be more effective at moving nuclei toward the microtubule plus-ends than the endogenous motor, likely due to loss of the autoinhibitory tail domain.

A conserved tryptophan-acidic motif in nesprin-2 localizes KLC to the nuclear envelope

The localization of Kif5B to the nucleus in myotubes is probably mediated by an interaction between KLCs and nesprins located on the outer NE (Wang et al., 2013b; Wilson and Holzbaur, 2012). In vertebrates, the tetratricopeptide repeat (TPR) domain of KLC binds directly to both nesprin-2 (Schneider et al., 2011; Wilson and Holzbaur, 2012) and nesprin-4 (Roux et al., 2009). In nesprin-2, this binding involves a conserved region located between spectrin repeats (SR) 53 and 54 (Schneider et al., 2011) (numbering according to Simpson and Roberts, 2008 based on the human Giant isoform) (Fig. 3A). This region, termed the 'adaptive domain', is predicted to contain a high degree of disordered loops and coils (Zhong et al., 2010). Within this region, there is an almost invariant ∼20-residue motif predicted to be a 'hot loop' or area of high mobility (Simpson and Roberts, 2008; Zhong et al., 2010). This adaptive domain and invariant motif are also found in nesprin-1 (located between SR71 and SR72), though the binding of KLC to nesprin-1 has not yet been reported. In nesprin-4, the KLC TPR domain has been shown to bind to the region between the SR and transmembrane domain (Roux et al., 2009) (Fig. 3A), a region that does not show obvious similarity to the adaptive domain of nesprin-2.

Within the highly conserved ∼20-residue motif in nesprin-1 and nesprin-2, we noticed a four-residue tryptophan-acidic (W-acidic) motif (Fig. 3B). This LEWD motif is similar to binding motifs described in other KLC-binding proteins (Aoyama et al., 2009; Dodding et al., 2011; Konecna et al., 2006; Schmidt et al., 2009). Analysis of the KLC-binding region of nesprin-4 also revealed the presence of the LEWD motif, though the flanking sequences were less conserved (Fig. 3B); this motif is absent from nesprin-3, which has not been reported to bind KLC.

To test the role of the LEWD motif, we performed co-immunoprecipitation experiments from COS7 cell lysates co-transfected with HA-KLC2 and the EGFP-tagged fragments of nesprin-2 (Fig. 3C). Although HA-KLC2 co-immunoprecipitated wild-type EGFP-nesprin-2 (6348-6552) and (6146-6799) fragments, mutating the WD residues in the LEWD motif to alanine residues (WD/AA) abolished this binding (Fig. 3D). This result indicates that the LEWD motif in nesprin-2 is a functional KLC-binding motif. To further verify this interaction, we performed additional co-immunoprecipitation experiments with HA-KLC2 constructs harboring point mutations in the WD-motif-binding groove shown to abrogate the binding of KLC2 to a SKIP peptide (SifA-kinesin interacting protein) containing a similar LEWD motif (TNLEWDDSAI) (Pernigo et al., 2013). Notably, the R251D mutation in the TPR2, and N287L and R312E mutations in the TPR3 domains of KLC2 significantly reduced light-chain binding to EGFP-nesprin-2 (6146-6799) (Fig. 3E,F) and a smaller nesprin-2 construct spanning residues 6348-6552 (supplementary material Fig. S3). Furthermore, when we expressed these HA-tagged KLC2 constructs in myotubes depleted of endogenous KLC1 and KLC2, wild-type HA-KLC2 showed clear accumulation around the nuclei, whereas the R251D, N287L and R312E mutations prevented this accumulation (Fig. 3G). Quantification of fluorescence intensity along a line spanning the nuclear membrane highlights the lack of recruitment of HA-KLC2 mutants to the NE compared with wild type (Fig. 3H).

Given the high sequence similarity between nesprin-1 and nesprin-2, it is likely that KLC2 also binds the LEWD motif in nesprin-1. Both nesprin-1 and nesprin-2 have a number of verified and suggested splice-isoforms with varied tissue distribution, but the LEWD motif is present in all but the shortest of the KASH domain-containing isoforms (Rajgor and Shanahan, 2013).

Mutations in KLC that disrupt binding to nesprins do not rescue nuclear positioning in myotubes

Kif5B is displaced from the nuclear envelope in myotubes treated with siRNA to KLC1 and KLC2 (Fig. 1D), and mutations in the KLC2 TPR domain prevent the localization of KLC to the NE (Fig. 3G). Therefore, we hypothesized that wild-type but not mutant KLC constructs would rescue the localization of Kif5B to the nucleus when expressed in myotubes lacking endogenous KLC1 and KLC2. In myotubes co-expressing EGFP-KLC2 WT and Myc-Kif5B-Halo in the absence of endogenous KLC, both of the tagged constructs localized to the NE (Fig. 4A,B). By contrast, Myc-Kif5B-Halo was not recruited to the nucleus in myotubes expressing any one of the three EGFP-KLC2 mutant constructs (Fig. 4A,B).

Development (2015) 142, 218-228 doi:10.1242/dev.114769

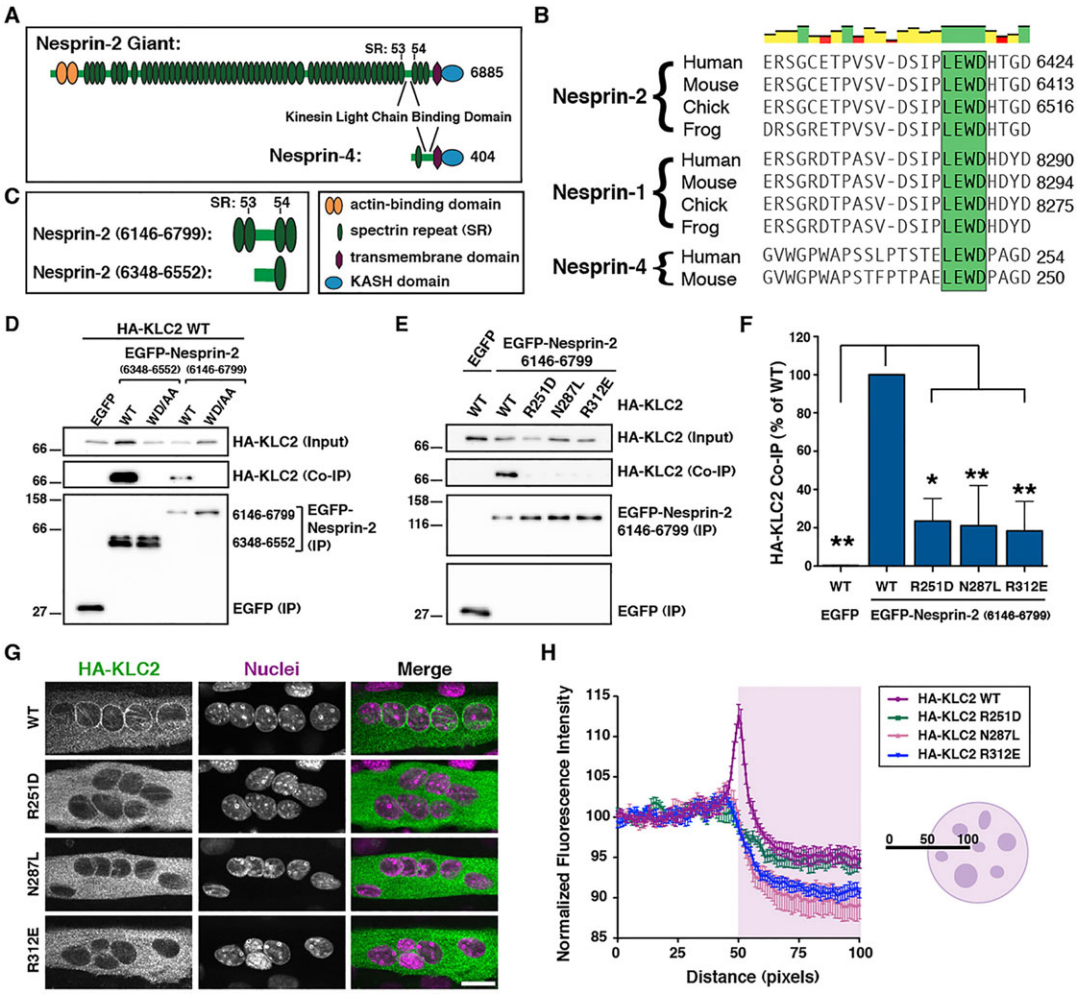

Fig. 3. A conserved W-acidic motif in nesprin-2 localizes KLC to the nuclear envelope. (A) Schematic of nesprin-2 Giant and nesprin-4 highlighting the previously mapped KLC-binding domains in each molecule (Roux et al., 2009; Schneider et al., 2011). (B) Alignment of nesprin sequences. The conserved LEWD motifs in nesprin-2, nesprin-1 and nesprin-4 are highlighted; numbering for nesprin-1 and nesprin-2 is based on the Giant isoform sequences; frog sequences are currently incomplete and have been left unnumbered; top panel indicates degree of conservation. (C) Schematic of the EGFP-tagged nesprin-2 fragments used in the following co-immunoprecipitation assays. (D) COS7 cells were transfected with HA-KLC2 and either wild-type EGFP-nesprin-2 fragments or EGFP-nesprin-2 fragments harboring WD/AA mutations in the LEWD motif. Immunoprecipitation of EGFP or EGFP-nesprin-2 constructs, followed by immunoblot analysis indicates that binding of KLC2 is abolished by mutations in the LEWD motif. (E) Co-immunoprecipitation experiments were performed using HA-KLC2 constructs with point mutations in the binding groove for the W-acidic motif. (F) Co-immunoprecipitation of HA-KLC2 R251D, N287L and R312E with EGFP-nesprin-2 (6146-6799) is significantly reduced (mean±s.e.m.; from n=3 independent experiments; ANOVA, *P<0.05, **P<0.01). (G,H) Myotubes were treated with siRNA to KLC1 and KLC2, and transfected with HA-KLC2 wild-type or mutant constructs. (G) Myotubes were stained for HA-KLC2. Scale bar: 20 µm. (H) As depicted, quantification of fluorescence intensity along a 100-pixel line centered at the NE was performed for the HA-KLC2 signal in these treated myotubes. Fluorescence intensity was normalized to the mean of the first 10 pixels of each line to account for variation in HA-KLC2 expression levels between myotubes (mean±s.e.m.; n=10 nuclei per condition from five myotubes). See supplementary material Fig. S3 for additional co-immunoprecipitation experiments.

Importantly, the TPR mutations in KLC2 do not disrupt binding of KLC to the Kif5B heavy chain (supplementary material Fig. S4). This suggests that functional motor complexes are still present, though they are unable to associate with the NE. When KLC1 and KLC2 siRNA-treated myotubes were transfected with HA-KLC2 R251D, N287L or R312E, nuclei continued to aggregate at the cell midline, whereas nuclei in cells expressing HA-KLC2 WT were distributed throughout the myotube (Fig. 4D,E,G). Although expression of HA-KLC2 WT restored the mean distance between adjacent nuclei to that of mock siRNA-treated myotubes (mock: 27±28 µm, n=389 nuclei in 51 myotubes versus WT: 26±31 µm, n=414 nuclei in 51 myotubes; mean±s.d.) (Fig. 4F), the distance between nuclei in the R312E mutant HA-KLC2 myotubes was not different from that in KLC1 and KLC2 siRNA-treated myotubes (R312E: 10±13 µm, n=542 nuclei in 54 myotubes versus KLC1 and KLC2: 10±11 µm, n=429 nuclei in 51 myotubes; mean±s.d.; Kruskal–Wallis test) (Fig. 4F). These findings again indicate that localization of Kif5B to the NE is necessary for proper nuclear distribution in developing muscle cells and that cytosolic localization of Kif5B is not sufficient.

Depletion of nesprins results in nuclear aggregation in myotubes

To test whether nesprins mediate the localization of kinesin-1 to the NE, we used siRNA against the 3′ untranslated regions (UTR) of nesprin-1 and nesprin-2 to deplete these proteins from myotubes. We confirmed knockdown of two isoforms of nesprin-1 (~110 and 120 kDa, likely the 1α isoforms) to 25±5% of mock (mean±s.d., n=3) (supplementary material Fig. S5A). Other nesprin-1 isoforms

Development (2015) 142, 218-228 doi:10.1242/dev.114769

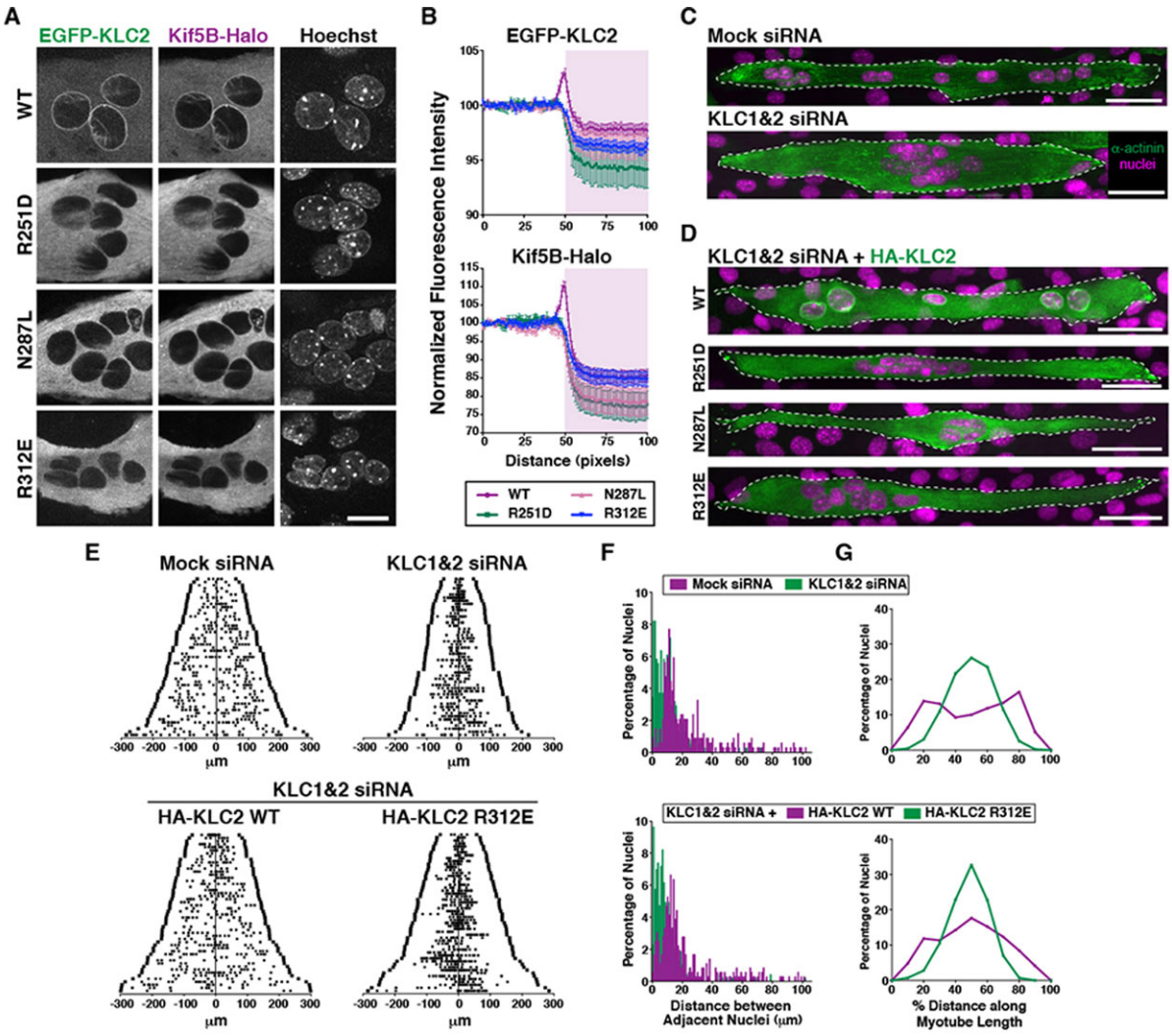

Fig. 4. Mutations in KLC that disrupt binding to nesprins do not rescue nuclear positioning in myotubes. (A,B) Myotubes were treated with siRNA to both KLC1 and KLC2, and transfected with EGFP-KLC2 WT, R251D, N287L or R312E and Myc-Kif5B-Halo. (A) The Halo tag was labeled with Halo-TMR ligand before image acquisition in live cells. Scale bars: 20 μm. (B) Quantification of fluorescence intensity along a 100-pixel line centered at the NE (as in Fig. 3H) was performed for the EGFP-KLC2 and Myc-Kif5B-Halo signals in these treated myotubes (mean±s.e.m.; *n*=10 nuclei per condition from five myotubes). (C) Representative images showing normal nuclear distribution in mock siRNA-treated myotubes compared with nuclear aggregation in KLC1 and KLC2 siRNA-treated myotubes. Images are maximum projections of confocal *z*-sections. Scale bars: 50 μm. (D) Myotubes were treated with siRNA to both KLC1 and KLC2, and transfected with HA-KLC2 WT, R251D, N287L or R312E constructs. Cells were stained for HA-KLC2 (green), KLC1 (see supplementary material Fig. S4) and nuclei (magenta). Only HA-KLC2 WT rescues the nuclear aggregation caused by loss of endogenous KLC1 and KLC2. Scale bars: 50 μm. (E) Distribution of nuclei in treated myotubes. Each line on the *y*-axis represents an individual myotube, organized according to length (*n*=51-54 myotubes). The ends of the myotube are marked by a dark square; data points represent individual nuclei. Only myotubes that lacked immunofluorescent staining for KLC1 were included in the analysis. (F) Frequency distributions of the distance between adjacent nuclei in treated myotubes (1 μm bin width; less than 2% of all the data lies above 105 μm so distributions are truncated for clarity). (G) Histograms depicting nuclear position as a percentage of the distance along the myotube length (bin width=10%). See also supplementary material Fig. S4 for supplemental data.

were likely reduced in parallel, but we were unable to confirm depletion of nesprin-2 isoforms.

siRNA-mediated depletion of nesprin-1 noticeably displaced EGFP-KLC2 and Myc-Kif5B-Halo from the NE (Fig. 5A,C). Nesprin-1-deficient myotubes exhibited aggregation of nuclei at the midline of the cell (Fig. 5D,F-H), similar to effects observed with either Kif5B or KLC siRNA (Figs 1B, 2 and 4). Analysis of the distance between adjacent nuclei confirmed the aggregation, as the distance was significantly reduced in nesprin-deficient myotubes compared with mock-treated cells (nesprin siRNA: 15±16 μm, *n*=383 nuclei in 56 myotubes versus mock siRNA: 25±21 μm, *n*=366 nuclei in 56 myotubes; mean±s.d.; $P<0.001$; Kruskal–Wallis with Dunn's post-hoc test; Fig. 5G, top panel).

Finally, to test whether the LEWD motif in nesprins mediates the binding of KLC to the NE in myotubes, we fused the short fragment of nesprin-2 containing the LEWD motif (6348-6552) to the KASH domain of nesprin-2 [EGFP-nesprin-2 (6348-6552)-KASH] and expressed this construct in myotubes with nesprin-1 depleted. Nuclei decorated with this construct recruited Myc-Kif5B-Halo to the NE, and the distribution of nuclei within these myotubes was rescued (Fig. 5B,C,E,G,H). However, mutation of the WD motif (WD/AA), prevented recruitment of Myc-Kif5B-Halo to the envelope and as a result nuclei remained aggregated at the midline (Fig. 5B,C,E,G,H). The mean distance between adjacent nuclei decorated with the wild-type construct is significantly greater than the distance between nuclei decorated with the WD/AA construct

Development (2015) 142, 218-228 doi:10.1242/dev.114769

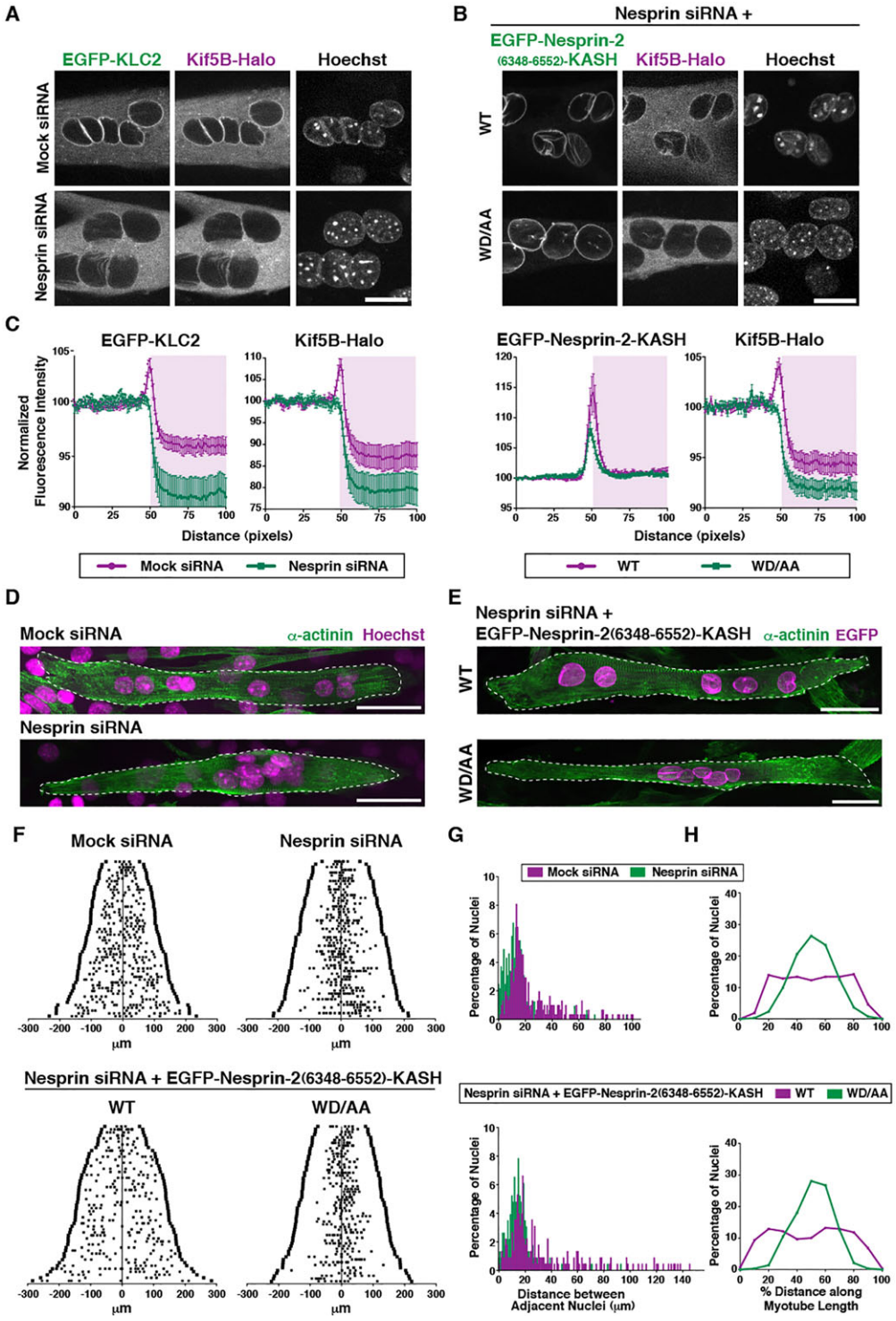

Fig. 5. Depletion of nesprins displaces Kif5B from the nuclear envelope and results in nuclear aggregation at the midline of the myotube. (A) Myotubes were treated with siRNA to the 3′UTR of nesprin-1 and nesprin-2, and transfected with EGFP-KLC2 and Myc-Kif5B-Halo. The Halo tag was labeled with Halo-TMR ligand before image acquisition in live cells. Scale bar: 20 µm. (B) Myotubes were treated with nesprin siRNA as in A, but were transfected with Myc-Kif5B-Halo and with EGFP-nesprin-2 (6348-6552)-KASH constructs containing either the wild-type sequence or the WD/AA mutation in the LEWD motif. Scale bar: 20 µm. (C) Quantification of fluorescence intensity along a 100-pixel line centered at the NE was performed (as in Fig. 3H) for the EGFP and Myc-Kif5B-Halo signals in myotubes treated as in A and B (mean±s.e.m.; n=10 nuclei per condition from five myotubes). (D) Representative images showing normal nuclear distribution in mock siRNA-treated myotubes compared with nuclear aggregation in nesprin-siRNA-treated myotubes. Images are maximum projections of confocal z-sections. Scale bars: 50 µm. (E) Myotubes were treated with nesprin siRNA and transfected with EGFP-nesprin-2 (6348-6552)-KASH constructs. Cells were stained for α-actinin (green) and EGFP (magenta). Only EGFP-nesprin-2 6348-6552-KASH WT rescues the nuclear aggregation caused by loss of endogenous nesprin-1. Scale bars: 50 µm. (F) Distribution of nuclei in treated myotubes. Each line on the y-axis represents an individual myotube, organized according to length (n=52-58 myotubes). The ends of the myotube are marked by a dark square; data points represent individual nuclei. (G) Frequency distributions of the distance between adjacent nuclei in treated myotubes [1 µm bin width; less than 2% of all the data lies above 105 µm (top) and 155 (bottom) so distributions are truncated for clarity]. (H) Histograms depicting nuclear position as a percentage of the distance along the myotube length (bin width=10%). See also supplementary material Fig. S5 for supplemental data.

Development (2015) 142, 218-228 doi:10.1242/dev.114769

(WT: 39±41 µm, n=279 nuclei in 52 myotubes versus WD/AA: 18±19 µm, n=288 nuclei in 58 myotubes; mean±s.d.; P<0.001; Kruskal–Wallis with Dunn's post-hoc test). Together, these data confirm that the LEWD motif of nesprin-1 and nesprin-2 mediates the association of kinesin-1 with the NE in developing myotubes and is required for normal nuclear positioning.

DISCUSSION

Here, using complementary experimental strategies, we provide evidence supporting the cargo-model of Kif5B-dependent nuclear movement in developing myotubes. We used an inducible dimerization system to specifically recruit Kif5B motors to the NE, and found that only nuclei with the HA-Kif5B-FRB motor construct bound escaped the nuclear aggregation that resulted from depletion of endogenous motor. In fact, HA-Kif5B-FRB-positive nuclei were often found at the extreme ends of myotubes (Fig. 2C,D), which are enriched in microtubule plus-ends (Wilson and Holzbaur, 2012). We speculate that this exaggerated distribution of HA-Kif5B-FRB-decorated nuclei relative to mock siRNA-treated myotubes reflects the constitutive activity of the truncated motor construct compared with the endogenous motor, which can be autoinhibited (Verhey and Hammond, 2009), and may be subject to regulation while bound to the NE.

We also show that depletion of KLC from the myotube displaces Kif5B from the NE, and results in nuclear aggregation at the cell midline. This positioning defect can be rescued by expression of wild-type KLC2, but not by KLC2 constructs with point mutations that prevent binding to nesprin-2. Depletion of nesprin-1 also displaces KLC and Kif5B from the NE, resulting in nuclear aggregation. Expression of EGFP-nesprin-2 (6348-6552)-KASH containing the LEWD motif rescues both the localization of Kif5B to the NE and nuclear distribution, whereas a WD/AA mutant that cannot bind KLC fails to rescue the defects. Together, these results argue that the nesprin-dependent recruitment of kinesin-1 to the NE is required to distribute nuclei along the myotube, supporting the cargo-model of kinesin-based nuclear movement.

Furthermore, these experiments argue against the microtubule-sliding model. In cells depleted of KLC or nesprin-1, Kif5B remains cytosolic, free to interact with MAP7. Mutations in the KLC TPR domain do not affect the binding of MAP7 to Kif5B (supplementary material Fig. S4D). However, nuclei aggregate at the cell midline under these conditions, indicating that, on its own, microtubule sliding by cytosolic Kif5B is unable to prevent nuclear aggregation. Although we cannot rule out a supporting role for Kif5B/MAP7-dependent microtubule sliding in nuclear distribution, this mechanism is not sufficient. In an alternative interpretation, MAP7 may contribute to the relief of kinesin-1 autoinhibition (Barlan et al., 2013), activating motors bound to the nucleus, which might account for the nuclear positioning defect noted in MAP7 mutant flies (Metzger et al., 2012).

Our results reveal that the W-acidic LEWD motif in the adaptive domains of nesprin-1 and nesprin-2 mediate binding to KLC2, and likely also to KLC1, as the TPR residues that mediate the binding interaction are conserved between these isoforms (Pernigo et al., 2013). mRNA for nesprin-2 giant and nesprin-2α1 account for ∼85% of nesprin-1 and nesprin-2 mRNA expressed in adult skeletal muscle (Duong et al., 2014), whereas nesprin-1 is more abundant in developing muscle cells (Randles et al., 2010). KLC is likely capable of binding all LEWD-containing nesprins, but accessibility of this site may be regulated *in vivo*. The shorter nesprin-1 and nesprin-2 isoforms are also found on the inner nuclear membrane in association with emerin and lamin A/C (Mislow et al., 2002; Wheeler et al., 2007), which may preclude their binding to kinesin. Finally, we speculate that the LEWD motif in nesprin-4, which is expressed in secretory epithelial cells (Roux et al., 2009) and the hair cells of the inner ear (Horn et al., 2013), mediates its known interaction with KLC.

Although our data indicate that nesprins serve as nuclear cargo adaptors for Kif5B motors, other NE proteins may also anchor the motor to the nucleus. As KLC2 R251D, N287L and R312E fail to localize to the NE (Figs 3G,H and 4A,B), other cargo adaptors likely interact via a tryptophan-acidic motif. One candidate is RanBP2, also known as Nup358, which serves as a kinesin-1 cargo adaptor for mitochondria (Cho et al., 2007). RanBP2 is also a component of the nuclear pore complex and recruits kinesin-1 to the nuclear surface specifically during the G2 phase of the cell cycle (Splinter et al., 2010). While RanBP2 interacts with the stalk and tail domains of Kif5B and Kif5C (Cho et al., 2007), the complex also includes KLC (Cai et al., 2001). We note that the kinesin-binding domain (KBD) of RanBP2 includes a LEWD motif, so KLC may also mediate the binding of kinesin-1 to RanBP2. In initial co-immunoprecipitation experiments, we find that HA-KLC2 binds RanBP2 KBD; the interaction is greatly diminished by the same TPR mutations that disrupt the localization of KLC2 to the NE (supplementary material Fig. S5B). Thus, RanBP2 may also act as a nuclear cargo adaptor for Kif5B in myotubes, although our observations indicate that depletion of nesprins was sufficient to block kinesin-1 recruitment in C2C12 cells (Fig. 5).

Previous work, based on overexpression of the KASH domain to displace endogenous nesprins, suggested that nesprins are not necessary for distributing nuclei in myotubes (Falcone et al., 2014; Metzger et al., 2012). In our system, siRNA-mediated depletion of nesprins reported here had a more substantial impact on nuclear distribution (Fig. 5) than overexpression of EGFP-nesprin-2-KASH (Wilson and Holzbaur, 2012), likely due to more effective displacement of kinesin-1 from the NE (Fig. 5). These cellular observations are consistent with data from transgenic mouse models, in which nuclear positioning defects are more severe upon targeted disruption or deletion of nesprin-1 isoforms (Chapman et al., 2014; Puckelwartz et al., 2009; Zhang et al., 2010, 2007b), when compared with deficits resulting from overexpression of KASH domains (Grady et al., 2005; Zhang et al., 2007b). In the latter mouse models, expression of the KASH domain did not completely displace endogenous nesprins (Grady et al., 2005; Zhang et al., 2007b). Under these circumstances, it is likely that the levels of Kif5B remaining on the NE following KASH overexpression are sufficient to properly distribute extrasynaptic nuclei. Going forward, it will be important to examine the effects of muscle-specific deletion of both nesprin-1 and nesprin-2 on nuclear positioning in order to understand whether nesprins are essential for distribution of extrasynaptic nuclei *in vivo*, and whether other cargo adaptors on the nucleus may compensate for the loss of nesprins.

Given that the localization of Kif5B to the NE is required for proper nuclear positioning, we propose that interactions of nuclear-based motors with the local microtubule network drives the nuclear dynamics observed in myotubes, including both translocation and rotation in three dimensions (Wilson and Holzbaur, 2012). For smaller cargoes, teams of kinesin-1 motors do not necessarily enhance velocity or travel distance of the organelle (Jamison et al., 2010; Shubeita et al., 2008). However, the large ensemble of Kif5B motors recruited to the nucleus by nesprins may be needed to produce the force necessary to move such a large organelle. The dynamics of individual nuclei are variable, with stochastic changes

Development (2015) 142, 218-228 doi:10.1242/dev.114769

in translational and rotational velocities and direction (Wilson and Holzbaur, 2012). This variability probably derives from the organization of the microtubule cytoskeleton surrounding the nucleus, which is highly dynamic (Wilson and Holzbaur, 2012), as well as the distribution and activity of the Kif5B on the envelope. Dynein is also located on the nuclear envelope in myotubes (Cadot et al., 2012; Wilson and Holzbaur, 2012) and would be expected to oppose the activity of kinesin-1, which may allow for more flexibility in moving such a large cargo through the complex cytoskeletal network in the developing myotube, similar to observations in *C. elegans* hypodermal cells (Fridolfsson and Starr, 2010). Unlike mouse myotubes, kinesin acts at the leading edge of the nucleus and dynein at the trailing edge in developing *Drosophila* muscles (Folker et al., 2014). This polarized distribution of motors may explain why nuclei in fly exhibit far less rotation than is observed in mouse cells.

We have shown using a number of experimental strategies that the ~10 µm wide nucleus can be considered a cargo for kinesin-1 in myotubes. By binding KLC via the LEWD motif, nesprins act as nuclear cargo adaptors for Kif5B, localizing the motor to the nuclear surface (Fig. 6). Achieving and maintaining proper nuclear positioning is not restricted to muscle fibers, but is crucial in diverse cell types, with aberrant positioning linked to dysfunction and disease (Gundersen and Worman, 2013). Given that the LEWD motif is found in multiple nesprin isoforms, our results suggest that nesprins mediate the localization of kinesin-1 to the NE in a wide variety of cells. Therefore, it will be important to learn how recruitment and activity of kinesin-1 on the NE is regulated in both developing and mature cells to allow for cell type-specific nuclear positioning.

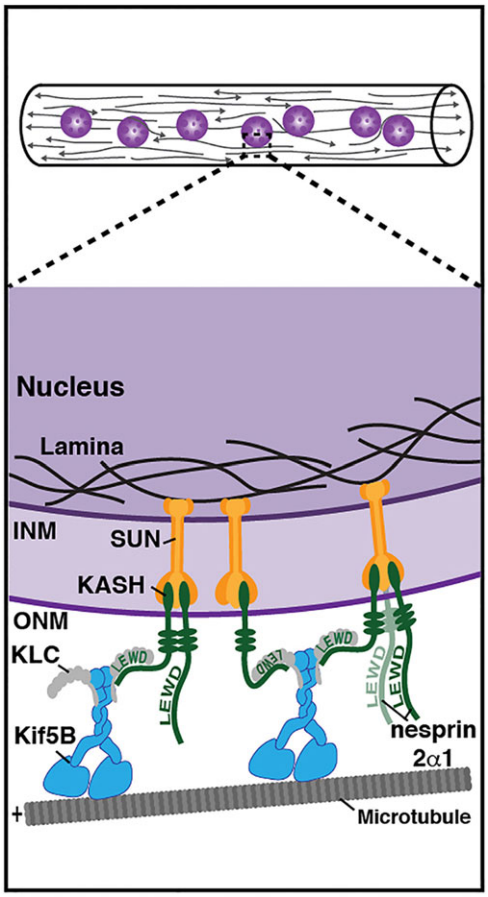

Fig. 6. Nesprins anchor kinesin-1 motors to the nucleus to drive nuclear distribution in muscle cells. Model with Kif5B motors anchored at the NE through an interaction between the TPR domain of KLC with the LEWD motif in nesprin-1 and nesprin-2 (only the short nesprin-2α1 isoform is depicted for clarity). Kif5B motors exert force on the local microtubule network to drive nuclear dynamics, allowing for proper distribution of nuclei throughout the developing myotube. ONM, outer nuclear membrane; INM, inner nuclear membrane.

MATERIALS AND METHODS

Reagents

The following constructs were generously provided: HA-Kif5B(1-807)-FRB and PEX3-mRFP-FKBP12 (human PEX3, Kif5B; Casper Hoogenraad, Utrecht University, The Netherlands); EGFP-nesprin-2α-KASH (human, residues 483-542; Catherine Shanahan, King's College London, UK); EGFP-nesprin-2 constructs (human, residues 6146-6799 and 6348-6552) (Angelika Noegel, University of Cologne, Germany); HA- and EGFP-tagged mouse KLC2 WT and R251D, N287L, R312E mutant constructs (Mark Dodding, King's College London, UK); pRK5-Myc-KifB and -Kif5C (mouse; Josef Kittler, University College London, UK); EGFP-MAP7 (mouse; Edgar Gomes, Pierre and Marie Curie University Paris, France); YFP-RanBP2-KBD (bovine, WT and KHC binding mutant KBD-mut1; Paulo Ferreira, Duke University School of Medicine, NC, USA).

FKBP-EGFP-KASH, Myc-Kif5B-Halo, EGFP-nesprin-2 (6146-7999) and (6348-6552) WD/AA mutants, and EGFP-nesprin-2 (6348-6552)-KASH (WT or WD/AA) constructs were generated in our laboratory. See supplementary material for details.

siRNA oligos to mouse Kif5B targeting a region in the tail domain of the mouse transcript absent from the truncated, human Kif5B(1-807) dimerization construct, and mouse KLC1, KLC2, nesprin-1 and nesprin-2 were from GE Healthcare Dharmacon. See supplementary material for details.

Primary antibodies include anti-GFP [GFP-1020, Aves Labs; immunofluorescence (IF) 1:1500, immunoblot (IB) 1:5000], anti-GFP [JL8, Clontech; IB 1:4000, immunoprecipitation (IP) 2.5 mg/50 ml beads], anti-GFP (ab1218, Abcam; IP 2.5 mg/50 ml beads), anti-Kif5B (ab15705, Abcam; IB 1:500), anti-a-actinin (clone EA-53, Sigma-Aldrich; IF 1:500), anti-KLC 1/2 (63-90, from Scott Brady, University of Illinois at Chicago, USA; IF 1:150, IB 1:500), anti-KLC1 (ab174273, Abcam; IF 1:400), anti-KHC (SUK4, Abcam; IF 1:200, IB 1:500), anti-GAPDH (mAb 9484, Abcam; IB 1:300), anti-HA (Covance; IF 1:1500, IB 1:2000-1:4000), anti-Myc (Ab 9106, Abcam; IB 1:1000, IP 2.5 mg/50 ml beads) and anti-actin (C4 clone, MAB1501, Millipore; IB 1:5000), anti-nesprin-1 and anti-nesprin-2 [from Didier Hodzic, Washington University in St Louis (Razafsky et al., 2013); IB 1:500 and 1:250, respectively). Alexa fluorophore-conjugated secondary antibodies and Hoechst 33342 (H21492) were from Molecular Probes (Invitrogen; IF 1:300-1:500). Cy2-conjugated goat anti-chicken antibodies (IF 1:500) and all HRP-conjugated secondary antibodies (IB 1:10,000) were from Jackson ImmunoResearch Laboratories.

C2C12 cell culture, transfections and ligand treatment

Mouse C2C12 myoblasts were maintained and differentiated as described (Wilson and Holzbaur, 2012). For immunofluorescence analyses, cells were grown on 1-cm^2 squares of ACLAR embedding film (Ted Pella) coated with 5 mg/cm^2 rat tail collagen, type 1 (BD Biosciences). For live cell imaging, cells were grown on 35 or 50 mm collagen-coated glass-bottomed dishes (FluorDish, World Precision Instruments). DNA transfections were performed with Lipofectamine 2000 (Invitrogen), and for RNAi, cells were transfected with siRNA Duplexes at a final concentration of 50 nM using Lipofectamine RNAiMax (Invitrogen). For motor recruitment assays, cells were tranfected with DNA ~84 h prior to cell fixation or live imaging and treated with siRNA ~12 h following DNA delivery. Control conditions were similarly treated with Lipofectamine 2000 and RNAiMax. For heterodimerization experiments, cells were treated with 500 nM A/C Heterodimerizer ligand (Clontech) starting 1 h after DNA transfection (nucleus) or with 1 mM ligand (peroxisomes) as noted in supplementary

Development (2015) 142, 218-228 doi:10.1242/dev.114769

material Fig. S1. For KLC and nesprin assays, cells were concurrently transfected with DNA and siRNA (KLC1 & KLC2 or nesprin-1 & -2 at 1:1 ratio) 72 h prior to cell fixation or live imaging. Labeling of cells transfected with Myc-Kif5B-Halo was performed with HaloTag TMR Ligand (Promega G8252) according to the manufacturer's instructions.

Immunofluorescence

Myotubes were fixed with 4% paraformaldehyde (PFA) and permeabilized with 0.1% Triton X-100, or fixed with ice-cold methanol with 1 mM EGTA when staining for kinesin-1. Fixed cells were incubated with primary and secondary antibodies, stained with Hoechst 33342 (0.5 µg/ml) and mounted on 40 mm glass coverslips with ProLong Gold antifade reagent (Invitrogen).

Co-immunoprecipitation and immunoblotting

COS7 cells (American Type Culture Collection, CRL-1651) were transfected using Fugene6 (Roche) according to the manufacturer's instructions and harvested 15-16 h after transfection. Two 10 cm plates of cells per condition were lysed with 300 µl ice-cold HEM [50 mM HEPES, 25 mM NaCl, 1 mM EDTA, 1 mM $MgCl_2$ (pH 7.0)] buffer with 0.1% Triton X-100 and protease inhibitor cocktail (Roche). Cells were sheared by five passages through a 20-gauge needle and incubated on ice for 30 min, followed by centrifugation at 13,000 ***g*** for 15 min at 4°C. The resulting supernatant was incubated for 60 min with Protein-G Dynabeads that were pre-incubated with either anti-HA (Covance) or anti-GFP (JL8, Clontech; ab1218, AbCam for EGFP-MAP7) antibodies. Beads were washed and boiled in 50 µl SDS-loading buffer. Samples were separated by SDS-PAGE, transferred to immobilon-PVDF membrane (Millipore) and subjected to immunoblotting. EGFP was detected using anti-EGFP raised in chicken (Aves Lab) to avoid detection of IgG bands.

siRNA knockdown of Kif5B and KLC was assessed by lysing cells in HEM buffer +1% Triton X-100 and protease inhibitor cocktail. Total protein was assessed using the BCA protein assay kit (Pierce) and equal total protein was subjected to immunoblot analysis. siRNA knockdown of nesprins was assessed by lysing the cells directly in 1× denaturing buffer supplemented with DNase and RNase, samples were boiled for 10 min at 95°C and equal volumes of lysate were subjected to immunoblot analysis. Equal loading was assessed by immunoblotting for GAPDH or actin.

Blots were visualized by detection of enhanced chemiluminescence (SuperSignal West Pico Chemiluminescent Substrate, Thermo Scientific) with the G:Box and GeneSys digital imaging system (Syngene). Densitometry was performed with Fiji (National Institutes of Health).

Microscopy

Fluorescence imaging was performed on a PerkinElmer UltraView Vox Spinning Disk Confocal with a Nikon Ti Microscope equipped with PFS, a motorized stage, and 40×/1.30 NA, 60×/1.49 NA and 100×/1.49 NA oil-immersion apochromatic objectives (Nikon). Digital images were acquired with a Hamamatsu EMCCD C9100-50 camera and Volocity 3D Image Analysis Software (Improvision/PerkinElmer). Live cell-imaging was performed in an environmental chamber set to 37°C; cells were imaged in Phenol Red-free DMEM with 25 mM HEPES (Gibco), 10% horse serum and 2 mM Glutamax. Where noted, DNA was labeled with Hoechst 33342 (0.5 mg/ml) for 20 minutes prior to imaging. Long-term imaging of PEX3-mRFP-FKBP in whole myotubes was performed at 40×, *z*-series encompassing the entire depth of each myotube (~20-30 mm, 1 mm *z*-step), were obtained every 15 minutes with from adjacent areas with 10% overlap. Images were stitched together digitally in Volocity to obtain composite images. Fast imaging of PEX3-mRFP-FKBP was performed 60× in a single *z*-plane at a rate of 20 frames/minute. Following labeling of the Halo-tag with TMR ligand, single *z*-plane images of EGFP-KLC2 and Myc-Kif5B-Halo-TMR were obtained in live cells at 60×. For analysis of nuclear distribution in whole myotubes, images of fixed cells were acquired at either 40× or 60×. *Z*-series encompassing the entire depth of each myotube (~15-30 mm) were taken at a step size of 1 or 2 mm. Adjacent areas were obtained with 10% overlap using the motorized stage. Images were stitched together digitally in Volocity to obtain composite images.

Image analysis

Nuclear distribution was assessed in stitched images of fixed myotubes using Volocity 3D Image Analysis Software. The ends of the myotubes and the centroid of each nucleus in the myotube was defined in XY; only unbranched myotubes <600 µm in length were included in the analysis. Nuclear position was linearized along the myotube length; distances between adjacent nuclei and nuclear position as a percent of the distance along the myotube length were calculated.

Line scan analyses were performed using Fiji. For details of the line scan analysis associated with Fig. 2, refer to supplementary material Fig. S2. For the line scan analyses in Figs 3, 4 and 5, a 100-pixel line was drawn from the cytoplasm into a nucleus at a right angle, such that the center of the line coincided with the edge of the nucleus, as demarcated by the Hoechst dye signal. The fluorescence intensity along this line was obtained in all pertinent channels. Data were normalized to the first 10 pixels of each line to account for variation in the cytoplasmic signal. All graphs and statistical analyses were performed using GraphPad Prism V5.0 (GraphPad Software). Figures were assembled using Fiji and Adobe Illustrator (Adobe).

Sequence alignments

Sequence alignments were performed in Geneious Basic 4.8.3 (Biomatters).

Acknowledgements

We gratefully acknowledge Mariko Tokito for technical assistance, Matthew Bray for development of Matlab scripts, Didier Hodic for the generous contribution of nesprin antibodies, Edward Ballister for helpful discussions regarding the inducible dimerization system, and Allison Twelvetrees for insight regarding kinesin-1. We also thank all members of the Holzbaur laboratory for helpful discussion and encouragement.

Competing interests

The authors declare no competing financial interests.

Author contributions

M.H.W. and E.L.F.H. designed experiments. M.H.W. performed experiments and analyzed the data. M.H.W. and E.L.F.H. wrote the manuscript.

Funding

This work was supported by the National Institutes of Health [PO1 GM087253 to E.L.F.H., T32 GM-07229 and T32 AR-053461 to M.H.W.] and the American Heart Association [#13PRE16090007 to M.H.W.]. Deposited in PMC for release after 12 months.

Supplementary material

Supplementary material available online at
http://dev.biologists.org/lookup/suppl/doi:10.1242/dev.114769/-/DC1

References

Aoyama, T., Hata, S., Nakao, T., Tanigawa, Y., Oka, C. and Kawaichi, M. (2009). Cayman ataxia protein caytaxin is transported by kinesin along neurites through binding to kinesin light chains. *J. Cell Sci.* **122**, 4177-4185.

Banerjee, I., Zhang, J., Moore-Morris, T., Pfeiffer, E., Buchholz, K. S., Liu, A., Ouyang, K., Stroud, M. J., Gerace, L., Evans, S. M. et al. (2014). Targeted ablation of nesprin-1 and nesprin-2 from murine myocardium results in cardiomyopathy, altered nuclear morphology and inhibition of the biomechanical gene response. *PLoS Genet.* **10**, pe1004114.

Barlan, K., Lu, W. and Gelfand, V. I. (2013). The microtubule-binding protein ensconsin is an essential cofactor of kinesin-1. *Curr. Biol.* **23**, 317-322.

Bruusgaard, J. C., Liestøl, K., Ekmark, M., Kollstad, K. and Gundersen, K. (2003). Number and spatial distribution of nuclei in the muscle fibres of normal mice studied in vivo. *J. Physiol.* **551**, 467-478.

Cadot, B., Gache, V., Vasyutina, E., Falcone, S., Birchmeier, C. and Gomes, E. R. (2012). Nuclear movement during myotube formation is microtubule and dynein dependent and is regulated by Cdc42, Par6 and Par3. *EMBO Rep.* **13**, 741-749.

Cai, Y., Singh, B. B., Aslanukov, A., Zhao, H. and Ferreira, P. A. (2001). The docking of kinesins, KIF5B and KIF5C, to Ran-binding protein 2 (RanBP2) is mediated via a novel RanBP2 domain. *J. Biol. Chem.* **276**, 41594-41602.

Capers, C. R. (1960). Multinucleation of skeletal muscle in vitro. *J. Biophys. Biochem. Cytol.* **7**, 559-565.

Chapman, M. A., Zhang, J., Banerjee, I., Guo, L. T., Zhang, Z., Shelton, G. D., Ouyang, K., Lieber, R. L. and Chen, J. (2014). Disruption of both nesprin-1 and

desmin results in nuclear anchorage defects and fibrosis in skeletal muscle. *Hum. Mol. Genet.* **23**, 5879-5892.
Cho, K.-i., Cai, Y., Yi, H., Yeh, A., Aslanukov, A. and Ferreira, P. A. (2007). Association of the kinesin-binding domain of RanBP2 to KIF5B and KIF5C determines mitochondria localization and function. *Traffic* **8**, 1722-1735.
Clackson, T., Yang, W., Rozamus, L. W., Hatada, M., Amara, J. F., Rollins, C. T., Stevenson, L. F., Magari, S. R., Wood, S. A., Courage, N. L. et al. (1998). Redesigning an FKBP-ligand interface to generate chemical dimerizers with novel specificity. *Proc. Natl. Acad. Sci. USA* **95**, 10437-10442.
Dodding, M. P., Mitter, R., Humphries, A. C. and Way, M. (2011). A kinesin-1 binding motif in vaccinia virus that is widespread throughout the human genome. *EMBO J.* **30**, 4523-4538.
Duong, N. T., Morris, G. E., Lam, L. T., Zhang, Q., Sewry, C. A., Shanahan, C. M. and Holt, I. (2014). Nesprins: tissue-specific expression of epsilon and other short isoforms. *PLoS ONE* **9**, e94380.
Englander, L. L. and Rubin, L. L. (1987). Acetylcholine receptor clustering and nuclear movement in muscle fibers in culture. *J. Cell Biol.* **104**, 87-95.
Falcone, S., Roman, W., Hnia, K., Gache, V., Didier, N., Lainé, J., Auradé, F., Marty, I., Nishino, I., Charlet-Berguerand, N. et al. (2014). N-WASP is required for Amphiphysin-2/BIN1-dependent nuclear positioning and triad organization in skeletal muscle and is involved in the pathophysiology of centronuclear myopathy. *EMBO Mol. Med.* **6**, 1455-1475.
Folker, E. S., Schulman, V. K. and Baylies, M. K. (2012). Muscle length and myonuclear position are independently regulated by distinct Dynein pathways. *Development* **139**, 3827-3837.
Folker, E. S., Schulman, V. K. and Baylies, M. K. (2014). Translocating myonuclei have distinct leading and lagging edges that require kinesin and dynein. *Development* **141**, 355-366.
Fridolfsson, H. N. and Starr, D. A. (2010). Kinesin-1 and dynein at the nuclear envelope mediate the bidirectional migrations of nuclei. *J. Cell. Biol.* **191**, 115-128.
Grady, R. M., Starr, D. A., Ackerman, G. L., Sanes, J. R. and Han, M. (2005). Syne proteins anchor muscle nuclei at the neuromuscular junction. *Proc. Natl. Acad. Sci. USA* **102**, 4359-4364.
Gundersen, G. G. and Worman, H. J. (2013). Nuclear positioning. *Cell* **152**, 1376-1389.
Horn, H. F., Brownstein, Z., Lenz, D. R., Shivatzki, S., Dror, A. A., Dagan-Rosenfeld, O., Friedman, L. M., Roux, K. J., Kozlov, S., Jeang, K. T. et al. (2013). The LINC complex is essential for hearing. *J. Clin. Invest.* **123**, 740-750.
Jamison, D. K., Driver, J. W., Rogers, A. R., Constantinou, P. E. and Diehl, M. R. (2010). Two kinesins transport cargo primarily via the action of one motor: implications for intracellular transport. *Biophys. J.* **99**, 2967-2977.
Kaan, H. Y. K., Hackney, D. D. and Kozielski, F. (2011). The structure of the kinesin-1 motor-tail complex reveals the mechanism of autoinhibition. *Science* **333**, 883-885.
Kapitein, L. C., Schlager, M. A., Kuijpers, M., Wulf, P. S., van Spronsen, M., MacKintosh, F. C. and Hoogenraad, C. C. (2010a). Mixed microtubules steer dynein-driven cargo transport into dendrites. *Curr. Biol.* **20**, 290-299.
Kapitein, L. C., Schlager, M. A., van der Zwan, W. A., Wulf, P. S., Keijzer, N. and Hoogenraad, C. C. (2010b). Probing intracellular motor protein activity using an inducible cargo trafficking assay. *Biophys. J.* **99**, 2143-2152.
Konecna, A., Frischknecht, R., Kinter, J., Ludwig, A., Steuble, M., Meskenaite, V., Indermühle, M., Engel, M., Cen, C., Mateos, J.-M. et al. (2006). Calsyntenin-1 docks vesicular cargo to kinesin-1. *Mol. Biol. Cell* **17**, 3651-3663.
Mattioli, E., Columbaro, M., Capanni, C., Maraldi, N. M., Cenni, V., Scotlandi, K., Marino, M. T., Merlini, L., Squarzoni, S. and Lattanzi, G. (2011). Prelamin A-mediated recruitment of SUN1 to the nuclear envelope directs nuclear positioning in human muscle. *Cell Death Differ.* **18**, 1305-1315.
Metzger, T., Gache, V., Xu, M., Cadot, B., Folker, E. S., Richardson, B. E., Gomes, E. R. and Baylies, M. K. (2012). MAP and kinesin-dependent nuclear positioning is required for skeletal muscle function. *Nature* **484**, 120-124.
Meyerzon, M., Fridolfsson, H. N., Ly, N., McNally, F. J. and Starr, D. A. (2009). UNC-83 is a nuclear-specific cargo adaptor for kinesin-1-mediated nuclear migration. *Development* **136**, 2725-2733.
Mislow, J. M. K., Holaska, J. M., Kim, M. S., Lee, K. K., Segura-Totten, M., Wilson, K. L. and McNally, E. M. (2002). Nesprin-1alpha self-associates and binds directly to emerin and lamin A in vitro. *FEBS Lett.* **525**, 135-140.
Pernigo, S., Lamprecht, A., Steiner, R. A. and Dodding, M. P. (2013). Structural basis for kinesin-1:cargo recognition. *Science* **340**, 356-359.
Puckelwartz, M. J., Kessler, E., Zhang, Y., Hodzic, D., Randles, K. N., Morris, G., Earley, J. U., Hadhazy, M., Holaska, J. M., Mewborn, S. K. et al. (2009). Disruption of nesprin-1 produces an Emery Dreifuss muscular dystrophy-like phenotype in mice. *Hum. Mol. Genet.* **18**, 607-620.
Rajgor, D. and Shanahan, C. M. (2013). Nesprins: from the nuclear envelope and beyond. *Expert Rev. Mol. Med.* **15**, e5.
Randles, K. N., Lam, L. T., Sewry, C. A., Puckelwartz, M., Furling, D., Wehnert, M., McNally, E. M. and Morris, G. E. (2010). Nesprins, but not sun proteins, switch isoforms at the nuclear envelope during muscle development. *Dev. Dyn.* **239**, 998-1009.
Razafsky, D. S., Ward, C. L., Kolb, T. and Hodzic, D. (2013). Developmental regulation of linkers of the nucleoskeleton to the cytoskeleton during mouse postnatal retinogenesis. *Nucleus* **4**, 399-409.
Romero, N. B. (2010). Centronuclear myopathies: a widening concept. *Neuromuscul. Disord.* **20**, 223-228.
Roux, K. J., Crisp, M. L., Liu, Q., Kim, D., Kozlov, S., Stewart, C. L. and Burke, B. (2009). Nesprin 4 is an outer nuclear membrane protein that can induce kinesin-mediated cell polarization. *Proc. Natl. Acad. Sci. USA* **106**, 2194-2199.
Schmidt, M. R., Maritzen, T., Kukhtina, V., Higman, V. A., Doglio, L., Barak, N. N., Strauss, H., Oschkinat, H., Dotti, C. G. and Haucke, V. (2009). Regulation of endosomal membrane traffic by a Gadkin/AP-1/kinesin KIF5 complex. *Proc. Natl. Acad. Sci. USA* **106**, 15344-15349.
Schneider, M., Lu, W., Neumann, S., Brachner, A., Gotzmann, J., Noegel, A. A. and Karakesisoglou, I. (2011). Molecular mechanisms of centrosome and cytoskeleton anchorage at the nuclear envelope. *Cell. Mol. Life Sci.* **68**, 1593-1610.
Shubeita, G. T., Tran, S. L., Xu, J., Vershinin, M., Cermelli, S., Cotton, S. L., Welte, M. A. and Gross, S. P. (2008). Consequences of motor copy number on the intracellular transport of kinesin-1-driven lipid droplets. *Cell* **135**, 1098-1107.
Simpson, J. G. and Roberts, R. G. (2008). Patterns of evolutionary conservation in the nesprin genes highlight probable functionally important protein domains and isoforms. *Biochem. Soc. Trans.* **36**, 1359-1367.
Spencer, D. M., Wandless, T. J., Schreiber, S. L. and Crabtree, G. R. (1993). Controlling signal transduction with synthetic ligands. *Science* **262**, 1019-1024.
Splinter, D., Tanenbaum, M. E., Lindqvist, A., Jaarsma, D., Flotho, A., Yu, K. L., Grigoriev, I., Engelsma, D., Haasdijk, E. D., Keijzer, N. et al. (2010). Bicaudal D2, dynein, and kinesin-1 associate with nuclear pore complexes and regulate centrosome and nuclear positioning during mitotic entry. *PLoS Biol.* **8**, e1000350.
Starr, D. A. and Fridolfsson, H. N. (2010). Interactions between nuclei and the cytoskeleton are mediated by SUN-KASH nuclear-envelope bridges. *Annu. Rev. Cell Dev. Biol.* **26**, 421-444.
Verhey, K. J. and Hammond, J. W. (2009). Traffic control: regulation of kinesin motors. *Nat. Rev. Mol. Cell Biol.* **10**, 765-777.
Verhey, K. J., Lizotte, D. L., Abramson, T., Barenboim, L., Schnapp, B. J. and Rapoport, T. A. (1998). Light chain-dependent regulation of Kinesin's interaction with microtubules. *J. Cell Biol.* **143**, 1053-1066.
Wang, Z., Cui, J., Wong, W. M., Li, X., Xue, W., Lin, R., Wang, J., Wang, P., Tanner, J. A., Cheah, K. S. E. et al. (2013a). Kif5b controls the localization of myofibril components for their assembly and linkage to the myotendinous junctions. *Development* **140**, 617-626.
Wang, Z., Xue, W., Li, X., Lin, R., Cui, J. and Huang, J.-D. (2013b). Dissect Kif5b in nuclear positioning during myogenesis: the light chain binding domain and the autoinhibitory peptide are both indispensable. *Biochem. Biophys. Res. Commun.* **432**, 242-247.
Wheeler, M. A., Davies, J. D., Zhang, Q., Emerson, L. J., Hunt, J., Shanahan, C. M. and Ellis, J. A. (2007). Distinct functional domains in nesprin-1alpha and nesprin-2beta bind directly to emerin and both interactions are disrupted in X-linked Emery-Dreifuss muscular dystrophy. *Exp. Cell Res.* **313**, 2845-2857.
Wilson, M. H. and Holzbaur, E. L. F. (2012). Opposing microtubule motors drive robust nuclear dynamics in developing muscle cells. *J. Cell Sci.* **125**, 4158-4169.
Zhang, Q., Bethmann, C., Worth, N. F., Davies, J. D., Wasner, C., Feuer, A., Ragnauth, C. D., Yi, Q., Mellad, J. A., Warren, D. T. et al. (2007a). Nesprin-1 and -2 are involved in the pathogenesis of Emery Dreifuss muscular dystrophy and are critical for nuclear envelope integrity. *Hum. Mol. Genet.* **16**, 2816-2833.
Zhang, X., Xu, R., Zhu, B., Yang, X., Ding, X., Duan, S., Xu, T., Zhuang, Y. and Han, M. (2007b). Syne-1 and Syne-2 play crucial roles in myonuclear anchorage and motor neuron innervation. *Development* **134**, 901-908.
Zhang, J., Felder, A., Liu, Y., Guo, L. T., Lange, S., Dalton, N. D., Gu, Y., Peterson, K. L., Mizisin, A. P., Shelton, G. D. et al. (2010). Nesprin 1 is critical for nuclear positioning and anchorage. *Hum. Mol. Genet.* **19**, 329-341.
Zhong, Z., Chang, S. A., Kalinowski, A., Wilson, K. L. and Dahl, K. N. (2010). Stabilization of the spectrin-like domains of nesprin-1alpha by the evolutionarily conserved "adaptive" domain. *Cell. Mol. Bioeng.* **3**, 139-150.